JMEPEG (2019) 28:2365–2377
https://doi.org/10.1007/s11665-019-04001-6

1059-9495/$19.00

Surface Structure and Corrosion Behavior of $Mg_{68-x}Zn_{28+x}Ca_4$ (x = 0.4) Bulk Metallic Glasses after Immersion in Ringer's Solution

Katarzyna Cesarz-Andraczke and Ryszard Nowosielski

(Submitted September 4, 2018; in revised form December 17, 2018; published online April 4, 2019)

The main aim of the present study was to determine the impact of Zn on the surface structure and corrosion behavior of Mg-based metallic glasses after immersion in Ringer's solution. The corrosion rate expressed by the volume of released hydrogen in the form of a function of immersion time in Ringer's solution at 37 °C was presented. The surface structure and corrosion products, which were formed during the immersion tests, were examined by means of scanning electron microscopy and the following spectroscopic methods: x-ray photoelectron spectroscopy, x-ray diffractometry, secondary ion mass spectrometry and energy-dispersive x-ray spectroscopy. As a result of the investigations of the surface structure, oxides (MgO, CaO, ZnO), hydroxides ($Mg(OH)_2$, $Ca(OH)_2$) and carbonates ($CaCO_3$) were identified. The analysis of the research results allowed the determination of a probable course and corrosion mechanism of the above-mentioned metallic glasses during immersion in Ringer's solution.

Keywords amorphous magnesium alloys, corrosion process, corrosion products, resorbable metallic alloys

1. Introduction

Recently, there has been an increasing interest in magnesium alloys as a material for resorbable short-term medical implants. A new concept of resorbable, orthopedic implants assumes that this new material with biocompatible elements will be resorbed after concrescence of the bone by the human body. This new concept is based on the combination of three factors: good bearing capacity of the implant (in accordance with sufficiently high mechanical strength), stable implant geometry (invariable during concrescence of the bone) and a controllable corrosion rate (dissolution rate).

In the subject literature, there is a lot of information about mechanical and corrosive properties of the above-mentioned Mg-based alloys with amorphous or crystalline structures, investigated in vivo (Ref 1, 2) and in vitro (Ref 3-5) conditions. However, one of the major issues connected with the concept of implants is a high quantity and intensity of hydrogen released during the corrosion process of magnesium alloys, which is too high and harmful to the human body. The mechanism of hydrogen release depends (among others) on pH solutions, the chemical composition of an alloy and the state of the implant surface. For example, previous in vitro investigations (Ref 6) showed that the solution used for corrosion containing phosphates decreased the release of hydrogen. On the other hand, chloride solutions are very aggressive in the case of in vitro corrosion studies, and very good for hard tests of implants. However, only few publications are accessible on this subject (Ref 7, 8). The corrosion investigations of magnesium-based metallic glasses were performed in Ringer's chloride solutions (8.6 g/dm^3 NaCl, 0.3 g/dm^3, KCI, 0.48 g/dm^3 $CaCl_2$ * $6H_2O$) at a temperature of 37 °C. The surface investigations after immersion tests for $Mg_{64}Zn_{32}Ca_4$ and $Mg_{68}Zn_{28}Ca_4$ metallic glasses were performed to determine the impact of Zn concentration on the surface structure and the course of corrosion process in Ringer's solution.

Katarzyna Cesarz-Andraczke and **Ryszard Nowosielski**, Institute of Engineering Materials and Biomaterials, Silesian University of Technology, Gliwice, Poland. Contact e-mail: Katarzyna.Cesarz-Andraczke@polsl.pl.

2. Materials and Methods

The studies of $Mg_{68}Zn_{28}Ca_4$ and $Mg_{64}Zn_{32}Ca_4$ metallic glasses in the form of cast rods were performed. Production of the samples of metallic glasses was conducted in two stages: preparation of a crystalline master alloy and casting of metallic glass samples in the form of rods (Ref 9, 10). Preparation of the master alloy was carried out by the induction melting of pure components: zinc (99.98%), magnesium (99.95%) and calcium (99.99%) in the argon atmosphere. In the second step, amorphous rods of a diameter of 2 mm were cast in a copper mold. Amorphous structures were identified by using a PANalytical X'Pert Pro x-ray diffractometer. Immersion tests and measurements of the released hydrogen volume of amorphous Mg-based alloys were carried out in Ringer's solution (8.6 g/dm^3 NaCl, 0.3 g/dm^3 KCl, 0.48 g/dm^3 $CaCl_2$ * $6H_2O$) for 336 h. Measurements of the hydrogen evolution volume were carried out at 37 °C by using an experimental station presented in the references (Ref 11, 12). The corrosion behavior was studied by electrochemical tests and mass loss method. Potentiodynamic corrosion studies in Ringer's solution at 37 °C using the Autolab potentiostat 302N, controlled by NOVA 1.11 software, were performed. The electrochemical cell of the potentiostat included work electrode—sample of magnesium alloy, counter platinum electrode and a reference

electrode—saturated calomel electrode (SCE). Before experiment, the samples were polished by a grinding paper with 1200 grains and subsequently cleaned in acetone. Also the mass loss of Mg-based metallic glasses after 2, 5, 10 h immersion was determined. The samples of studied alloys before and after immersion in Ringer's solution were weighed. The samples' surface before weighing, in chromic acid anhydride with 99.99% purity in 25 °C during 30 min, was cleaned. The structure and chemical composition of the layer of corrosion products were studied by means of the scanning electron microscopy/energy-dispersive x-ray spectroscopy (SEM/EDS), x-ray photoelectron spectroscopy (XPS), x-ray diffractometry (XRD) and secondary ion mass spectrometry (SIMS).

3. Results

X-ray diffraction studies have confirmed that $Mg_{68}Zn_{28}Ca_4$ and $Mg_{64}Zn_{32}Ca_4$ rods with a 2 mm diameter have an amorphous structure. The fuzzy spectrum in the range of 38°-52°, which is characteristic of amorphous structure, was determined for all samples (Fig. 1).

The results of immersion tests of $Mg_{68-x}Zn_{28+x}Ca_4$ (x = 0.4) alloys in Ringer's solution at 37 °C (Fig. 2) present the volumes of hydrogen evolution during 2 weeks (336 h). The highest amount of released hydrogen, that is about 1.93 mL/cm^2 for the $Mg_{68}Zn_{28}Ca_4$ alloy, was determined. The lowest amount of released hydrogen, that is about 1.21 mL/cm^2 for the $Mg_{64}Zn_{32}Ca_4$ alloy, was determined. For all investigated magnesium alloys, the largest volume of released hydrogen for the first 3-4 h of immersion in Ringer's solution was found. With the increase in the immersion time (up to 24 h of immersion), the released hydrogen was unmeasurable (the level of the solution in the burette did not change). Additionally, the chart of immersion tests presents the results obtained for all tested alloys and alternately shows periodic intervals with large and small (almost zero) rates of released hydrogen. The structure of corrosion products, which were formed during the immersion tests on the sample surface, was examined by scanning electron microscopy. After 5, 10 and 24 of immersion in Ringer's solution, the layers of corrosion products were formed on the surface of $Mg_{68}Zn_{28}Ca_4$ and $Mg_{64}Zn_{32}Ca_4$ samples. After 10 and 24 h (Fig. 3c, d, e and f) of immersion, the corrosion products layer on the surface of sample $Mg_{64}Zn_{32}Ca_4$ may be more compact in comparison with the corrosion products layer on the surface of the $Mg_{68}Zn_{28}Ca_4$ sample. After 24 h of immersion, on the surface of the $Mg_{68}Zn_{28}Ca_4$ alloy, there appeared elements in the shape of needles. After 24 h (Fig. 3e and f) of immersion, on the surface of alloy $Mg_{64}Zn_{32}Ca_4$ there were elements in the shape of petals. The results of the EDX chemical composition indicated that these needle-shaped and petal-shaped elements consisted mainly of zinc, oxygen and a small concentration of magnesium. Furthermore, the chemical composition analysis of corrosion products before and after 5, 10, 24 h of immersion (Table 1) for both tested metallic glasses showed a large concentration (wt.%) of Zn and a decreasing concentration of Ca (wt.%).

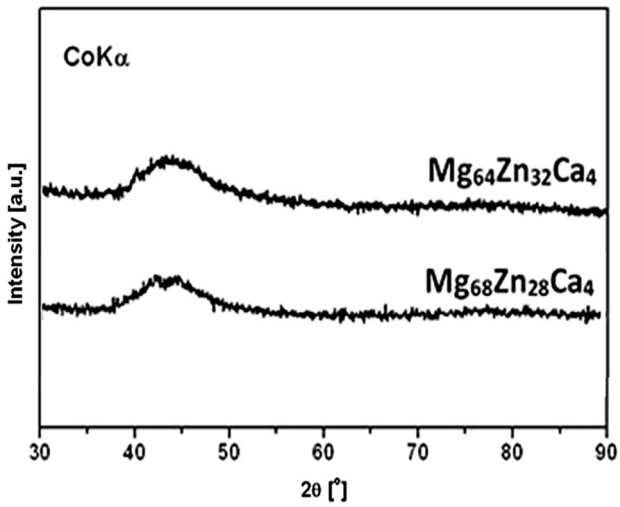

Fig. 1 X-ray diffraction patterns of $Mg_{68-x}Zn_{28+x}Ca_4$ (x = 0.4) alloys in the form of rods with a diameter of 2 mm

After 336 h of immersion, the surface of the $Mg_{68}Zn_{28}Ca_4$ sample was coated with a thick and dense layer of calcium carbonate (Fig. 4). The surface of the $Mg_{64}Zn_{32}Ca_4$ sample was coated with a tiny calcium carbonate precipitate, sometimes with a spherical shape (Fig. 5). After 336-h immersion of $Mg_{68}Zn_{28}Ca_4$ and $Mg_{64}Zn_{32}Ca_4$ samples, they were compared with the chemical composition of the surface after 168 h of immersion (Table 2). A large concentration of O, C and Ca on the samples' surface was observed.

A chemical composition of the surface of the $Mg_{64}Zn_{32}Ca_4$ alloy was also performed by x-ray photoelectron spectroscopy. The XPS results (Fig. 6) and high-resolution spectra of the C1s lines (Fig. 7) indicated the presence of MgO, $Mg(OH)_2$, $Ca(OH)_2$,CaO, ZnO and $CaCO_3$ on the $Mg_{64}Zn_{32}Ca_4$ samples surface after 1 day, 1 week and 2 weeks of immersion.

In addition XRD studies (Fig. 8) of layers of corrosion products for both tested alloys were carried out, which also indicate the presence of calcium carbonate.

In addition, another parallel corrosion tests were carried out as electrochemical and weight loss methods. After 2-h immersion, indiscernible weight loss (Table 3 and Fig. 9) for all tested metallic glasses was observed. After 5- and 10-h immersion, the weight loss (Fig. 9) increases for all tested metallic glasses. The increasing of weight loss maybe caused the formation of the surface samples corrosion product' layers, which caused samples partially dissolved. This is confirmed by the corrosion product' images on the surface of samples $Mg_{68}Zn_{28}Ca_4$ and $Mg_{64}Zn_{32}Ca_4$ alloys (Fig. 5). The current density of $Mg_{68}Zn_{28}Ca_4$ and $Mg_{64}Zn_{32}Ca_4$ alloys after 15-min and 10-h immersion is lower than after 2- and 5-h immersion during the process of cathodic polarization (Fig. 10). It means that after 15-min and 10-h immersion $Mg_{68}Zn_{28}Ca_4$ and $Mg_{64}Zn_{32}Ca_4$ alloys are less cathodically active (less released hydrogen) than after 2- and 5-h immersion in Ringer's solution. It is correlated with immersion tests results, where in $Mg_{68}Zn_{28}Ca_4$ and $Mg_{64}Zn_{32}Ca_4$ alloys during 5- to 10-h immersion the smallest hydrogen was released.

In addition, corrosion rate (V_{corr}) determined by electrochemical tests (Table 3) after 5- and 10-h immersion increases insignificantly for both studied alloys. Probably it can be associated with some stabilization of the corrosion products layers was so compact that it hindered the release of hydrogen and release of elements ions.

However, after 10-h immersion corrosion rate in mm/year determined by weight loss and determined by electrochemical

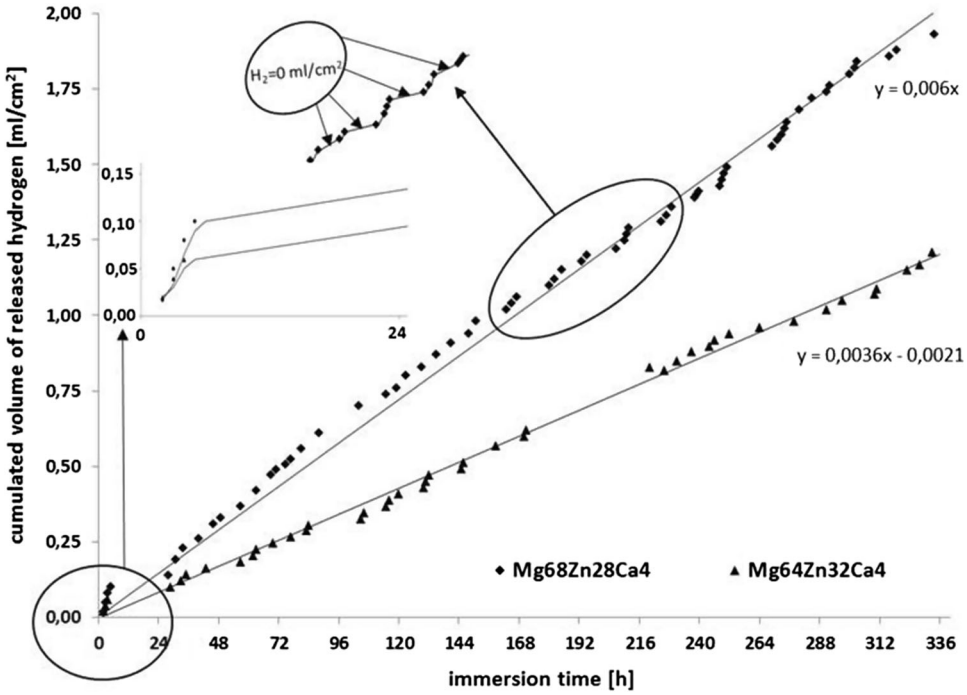

Fig. 2 Cumulated volume of released hydrogen of studied $Mg_{68-x}Zn_{28+x}Ca_4$(x = 0.4) metallic glasses immersed in Ringer's solution at 37 °C

tests is different (Table 3). The contradiction between this corrosion tests results may be associated with a layer of corrosion product, which removed to determine the weight loss rate and did not remove to measure current density by electrochemical tests. During polarization, the dissolution of sample is accelerated, which can prevent the formation of a corrosion product layer, which during immersion test was established naturally.

The results of the SIMS studies (Fig. 11 and 12) confirmed inhomogeneous location of corrosion products on the surface of $Mg_{68}Zn_{28}Ca_4$ and $Mg_{64}Zn_{32}Ca_4$ samples. In the micro-area of the $Mg_{68}Zn_{28}Ca_4$ sample after 24 h of immersion in Ringer's solution (Fig. 11), magnesium ions were localized in the major part of the area. Calcium and zinc ions were localized in small-spot regions. In the micro-area of the $Mg_{64}Zn_{32}Ca_4$ sample after 24 h of immersion in Ringer's solution (Fig. 12), magnesium ions were localized in the upper left-hand corner and bottom right-hand corner (Fig. 12a). The calcium and zinc ions were localized in small micro-areas (Fig. 12c and d).

4. Discussion

The layer of corrosion products probably isolated at least a part of the metallic surface from the solution, and in consequence decreased the corrosion rate. This phenomenon may be related to the destruction and rebuilding of the layer of corrosion products during the immersion of samples in Ringer's solution. After 5 h of immersion in Ringer's solution on the surface of $Mg_{68}Zn_{28}Ca_4$ and $Mg_{64}Zn_{32}Ca_4$ samples (Fig. 3a and b), a corrosion products layer was formed. The decrease in the released hydrogen after 5 h of immersion may have been caused by the formation of a layer of corrosion products on the samples' surface. It could confirm the above-mentioned hypothesis that layers of corrosion products have an impact on the corrosion rate change and cause passive-like intervals. Such a corrosion behavior of $Mg_{68}Zn_{28}Ca_4$ metallic glass in the present work correlates with the results present by Wang et al. (Ref 13) for the amorphous $Mg_{67}Zn_{28}Ca_5$ alloy. This is also confirmed by the results obtained by Zberg et al. (Ref 14), who found that when the concentration of zinc in the alloy exceeds 28 at.% the formation of the layer of corrosion products is possible. Artens et al. (Ref 15) also performed the measurement of released hydrogen volume and determined the dissolution rate of $Mg_2Zn_{0.2}Mn$, ZE41, AZ91 alloys and high-purity Mg samples. For each sample, except Mg the incubation period with very low (near zero) hydrogen released was observed. In the work (Ref 13) found, that the decreasing of released hydrogen rate, it could be related to the destruction and regrowth layer of corrosion products during immersion samples of alloys in solution. This is confirmed by results of corrosion products layers studies on samples (Fig. 3, 4 and 5) after immersion, which indicated continuous changes in morphology, cohesion and chemical composition of layers.

In addition, in this work it is confirmed by corrosion products on samples of studied alloys (Fig. 3c, d, e and f) after 10- and 24-h immersion, which ensured probably effective protection against the release of hydrogen. On the other hand, large amounts of calcium ions (Table 1) in the solution resulted in the $Mg_{68}Zn_{28}Ca_4$ sample dissolution. Presence of carbon compounds and Ca ions in the solution resulted in the precipitation of a solid calcium carbonates layer (Fig. 4a). After 2 weeks of immersion of $Mg_{68}Zn_{28}Ca_4$ and $Mg_{64}Zn_{32}Ca_4$ samples (Table 2), a large concentration of O, C and Ca was observed on the sample surface. Probably, it was associated with the calcium carbonate layer which also precipitated on the sample surface. The calcium carbonate found on the surface

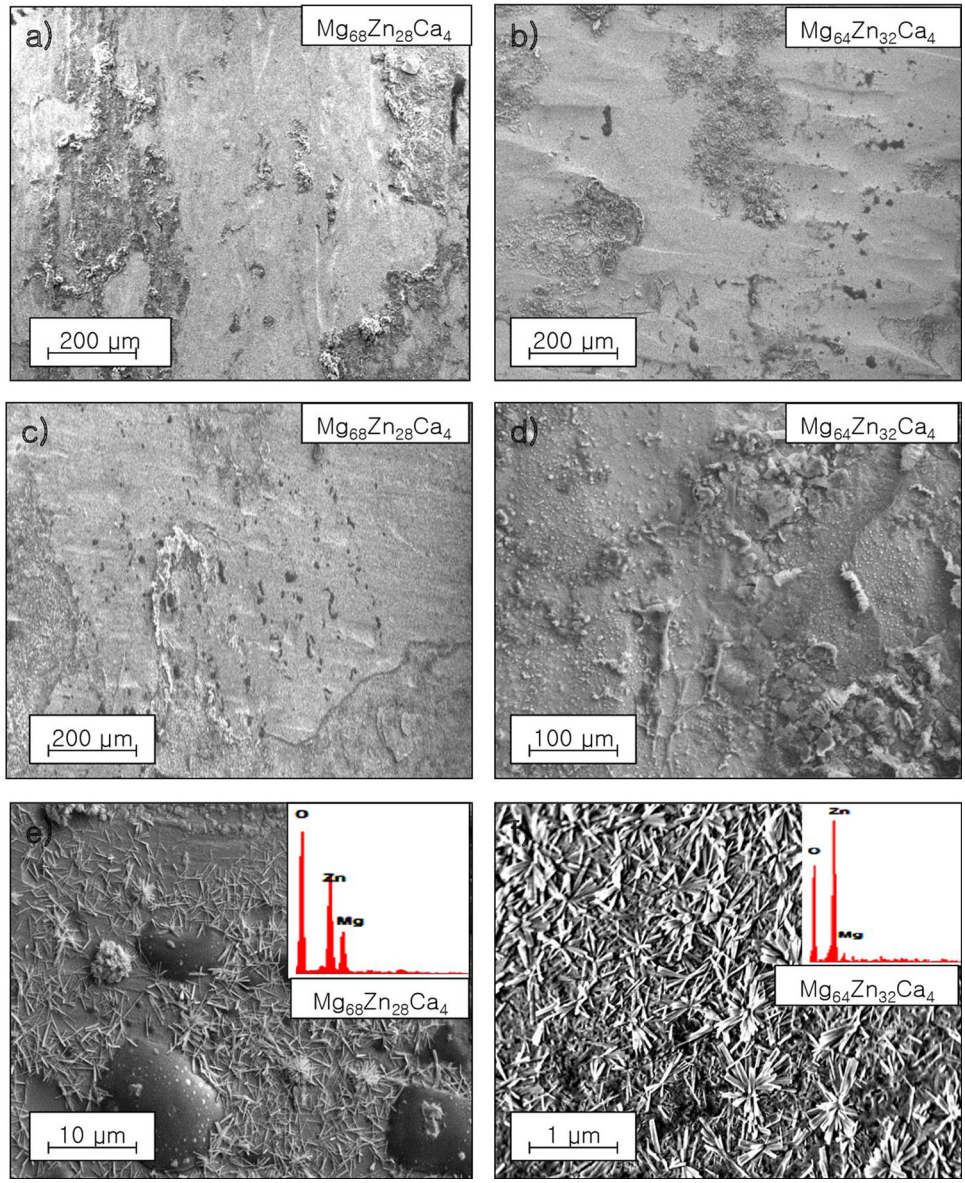

Fig. 3 Surface structure (SEM) of $Mg_{68}Zn_{28}Ca_4$ and $Mg_{64}Zn_{32}Ca_4$ samples after: (a, b) 5-h immersion, (c, d) 10-h immersion and (e, f) 24-h immersion in Ringer's solution at 37 °C

Table 1 Results of the analysis of chemical composition (EDS): $Mg_{64}Zn_{32}Ca_4$ and $Mg_{68}Zn_{28}Ca_4$ samples before and after 5, 10 and 24 h of immersion in Ringer's solution at 37 °C

	Elements, at.%					Mg, Zn, Ca, wt.%		
Time	**O**	**Cl**	**Mg**	**Zn**	**Ca**	**Mg**	**Zn**	**Ca**
$Mg_{68}Zn_{28}Ca_4$								
Before immersion	1.36	…	66.3	28.11	4.23	44.25	50.48	4.65
After 5-h immersion	50.73	1.57	28.02	16.66	3.02	24.68	39.48	4.38
After 10-h immersion	48.87	3.34	31.15	14.42	2.22	28.83	35.91	3.38
After 24-h immersion	65.11	0.30	25.22	7.54	1.83	27.46	22.09	3.28
$Mg_{64}Zn_{32}Ca_4$								
Before immersion	3.54	…	60.76	30.90	4.79	39.42	53.93	5.12
After 5-h immersion	50.25	1.18	33.25	12.99	2.32	31.13	32.71	3.58
After 10-h immersion	56.19	0.94	26.37	14.62	1.88	24.62	36.70	2.89
After 24-h immersion	82.11	…	6.63	20.47	…	6.02	50.60	…

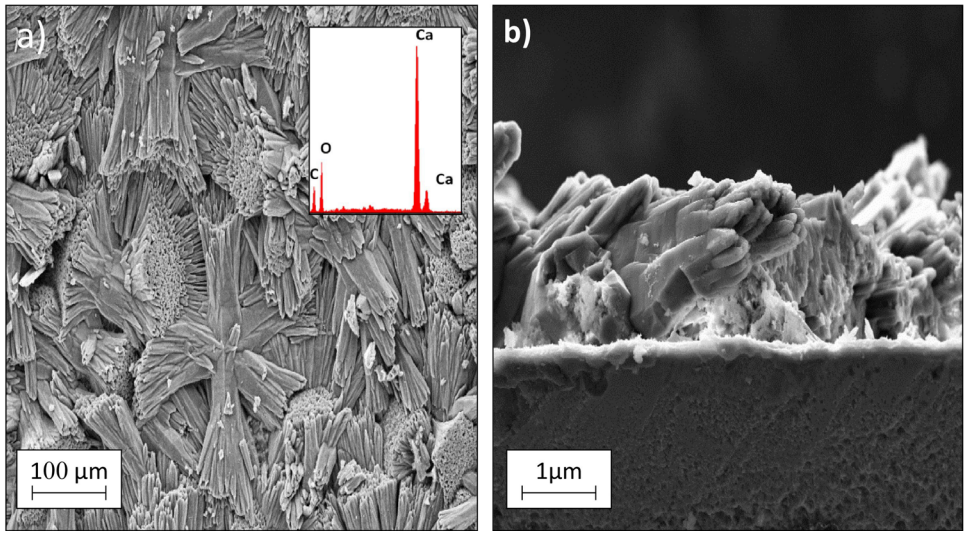

Fig. 4 Surface structure (a) and fracture of the $Mg_{68}Zn_{28}Ca_4$ sample with the layer of corrosion products (b) after 336-h immersion in Ringer's solution at 37 °C (SEM)

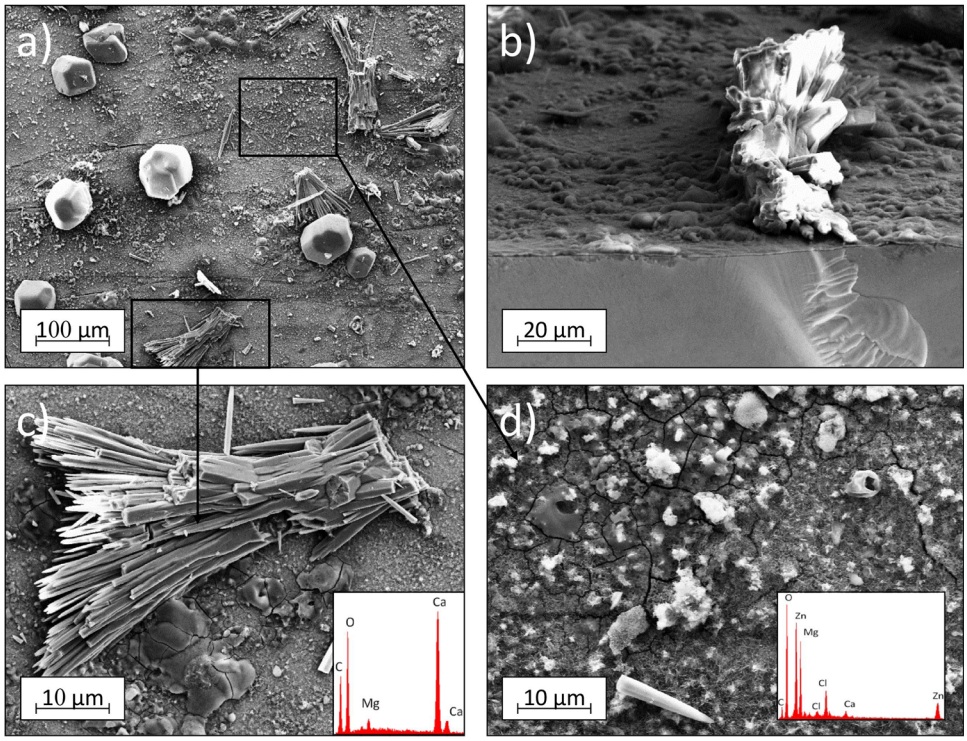

Fig. 5 Surface structure (a, c, d) and fracture of the $Mg_{64}Zn_{32}Ca_4$ sample with the layer of corrosion products (b) after 336-h immersion in Ringer's solution at 37 °C (SEM)

Table 2 Results of the analysis of chemical composition (EDS): $Mg_{64}Zn_{32}Ca_4$ and $Mg_{68}Zn_{28}Ca_4$ samples before and after 168 and 336 h of immersion in Ringer's solution at 37 °C

	Elements, at.%						Mg, Zn, Ca, wt.%		
Time	**C**	**O**	**Cl**	**Mg**	**Zn**	**Ca**	**Mg**	**Zn**	**Ca**
$Mg_{68}Zn_{28}Ca_4$									
After 168-h immersion	11.53	45.53	6.35	32.55	3.02	1.02	37.30	69.72	2.92
After 336-h immersion	26.31	52.07	…	…	…	21.62	…	…	42.98
$Mg_{64}Zn_{32}Ca_4$									
After 168-h immersion	59.95	4.64	…	1.17	32.04	2.19	0.94	32.06	2.92
After 336-h immersion (Fig. 9d)	32.21	41.28	…	…	–	38.51	…	…	18.40

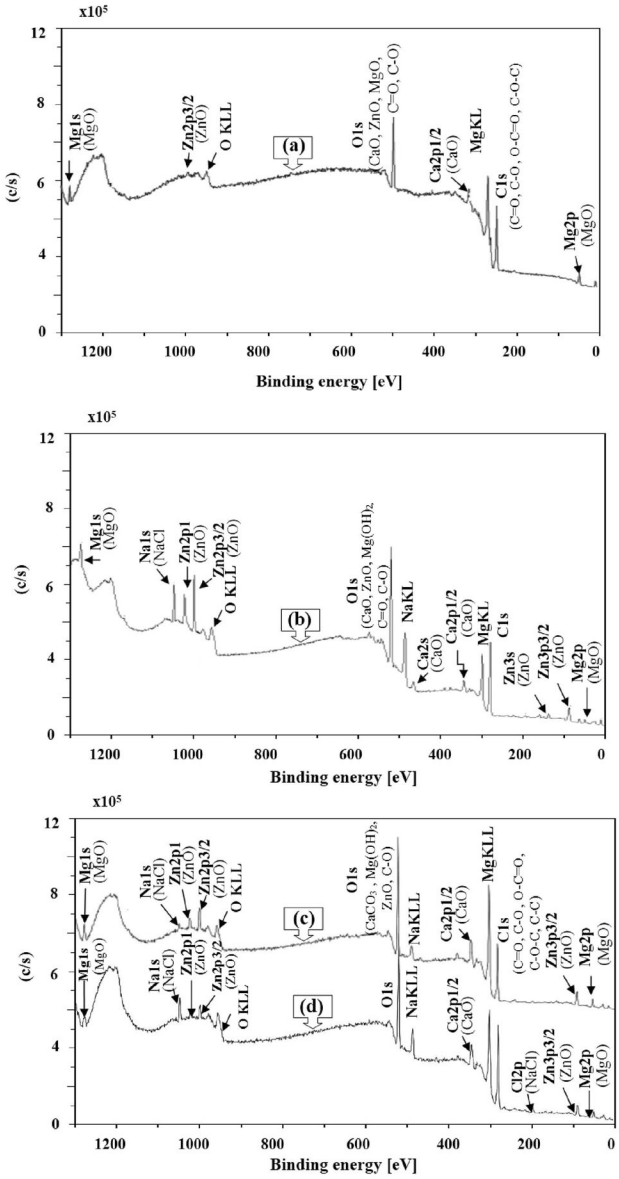

Fig. 6 XPS spectra of $Mg_{64}Zn_{32}Ca_4$ samples: (a) before immersion, (b) after 24 h, (c) after 1 week of immersion and (d) after 2 weeks of immersion in Ringer's solution at 37 °C (the chemical state based on the analysis of high-resolution spectrum has been indicated in brackets)

(Fig. 6d) of studied samples may have precipitated as a result of the reaction of calcium ions from the dissolution of metals with carbon dioxide from the air. The calcium carbonate of particles in the solution was precipitated from the solution on the samples' surface creating an anticorrosive layer. The $CaCO_3$ layer was stable at an alkaline pH of the solution (Ref 16). The solution with an alkaline pH was mainly produced by the released hydrogen and the formation of hydroxyl groups (OH) (Ref 17). Therefore, it can be assumed that a larger volume of released hydrogen may cause a more compact layer of the calcium carbonate. The presence of calcium carbonate in the layer indicates the results of XRD (Fig. 8). This hypothesis has been partly confirmed by the results of immersion tests (Fig. 2). The volume of released hydrogen after 2 weeks of immersion of the $Mg_{68}Zn_{28}Ca_4$ sample in Ringer's solution was nearly twice as high as the volume of released hydrogen during the immersion of the $Mg_{64}Zn_{32}Ca_4$ sample. A higher concentration of zinc in the $Mg_{64}Zn_{32}Ca_4$ alloy caused lower hydrogen evolution and less calcium carbonate in the surface structure after the immersion test. It should be noted that the $CaCO_3$ precipitate does not need to form in the human organism because there is a flow of body fluids which makes it difficult to precipitate. Based on the surface studies of $Mg_{64}Zn_{32}Ca_4$ metallic glass, the structure and chemical composition of corrosion products are determined and shown in Fig. 13.

On the basis of the results obtained from corrosion studies of Mg-based metallic glasses, it is possible to distinguish generally five stages of the corrosion process in Ringer's solution:

- Transformation of an oxide layer into a hydroxide layer.
- Penetration of chlorides into the hydroxide layer.
- Release of metal ions and penetration into the solution.
- Release of hydrogen.
- Formation of a protective layer.

It should be noted that the stages do not follow each other, but can occur simultaneously during the immersion of Mg-based metallic glasses. It may be associated with the inhomogeneous location of corrosion products on the surface of the samples. This fact is confirmed by the results of the SIMS studies (Fig. 11 and 12) and the SEM images (Fig. 3, 4 and 5) of the surface after immersion tests.

Transformation of an oxide layer into a hydroxide layer When the Mg-based metallic glass was immersed, the process of dissolution began on the samples' surface. The surface of sample $Mg_{64}Zn_{32}Ca_4$ was coated with an oxide layer before

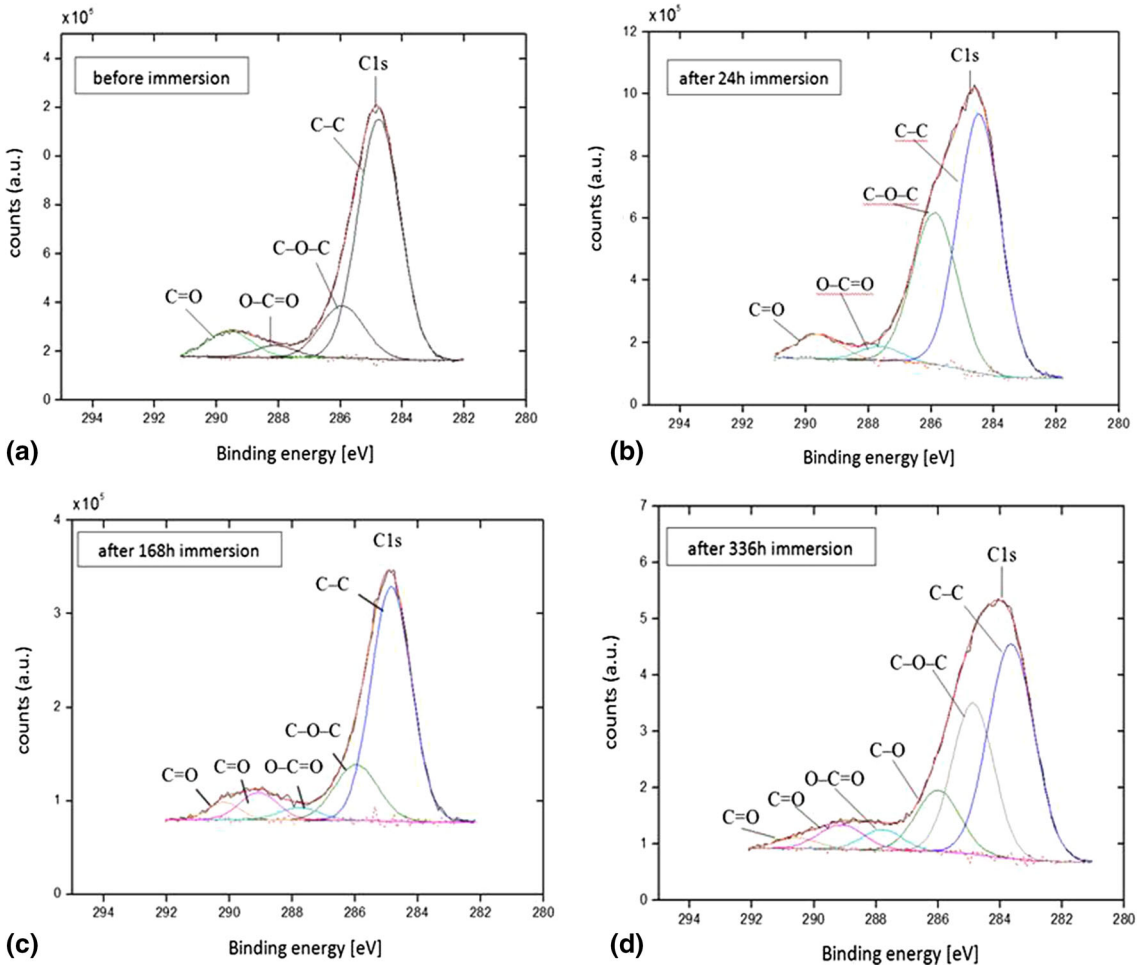

Fig. 7 High-resolution spectra of the C1s lines: (a) before immersion, (b) after 24-h immersion, (c) after 168-h immersion and (d) after 336-h immersion in the Ringer solution of the $Mg_{64}Zn_{32}Ca_4$ alloy

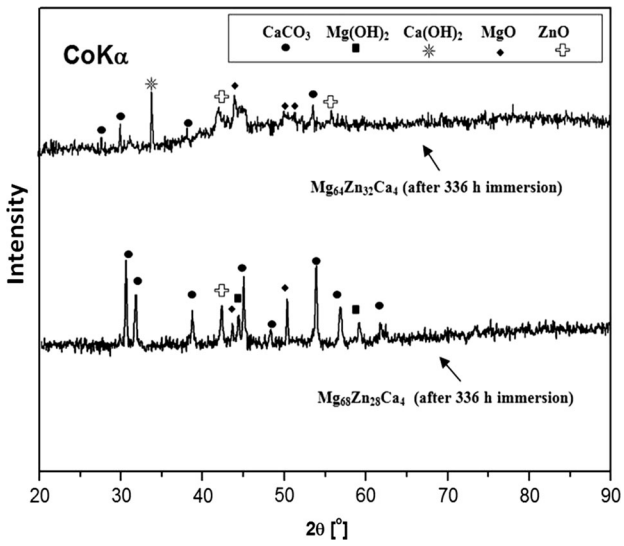

Fig. 8 X-ray diffraction of dissolution products from the surface of $Mg_{68}Zn_{28}Ca_4$ and $Mg_{64}Zn_{32}Ca_4$ alloys

immersion (Table 1). The oxide layer on magnesium alloys was porous and discontinuous. The Pilling–Bedworth's ratio for magnesium oxide was 0.81. It means that the oxide layer on magnesium alloys was leaky (Ref 18). The oxide layers on magnesium alloys had several nanometers of thickness (Ref 19).The Santamaria et al. (Ref 20) found that oxide layer on the magnesium with a thickness of 2.2 nm included MgO and $Mg(OH)_2$. After immersion in aqueous Ringer's solution, the oxide layer on Mg-based metallic glasses was transformed into a hydroxide layer by reactions 1 and 2:

$$MO + H_2O \rightarrow M(OH)_2 (M = Ca, Mg) - \text{reaction in areas with the oxide layer} \quad \text{(Eq 1)}$$

$$M + H_2O \rightarrow M^{2+} + 2OH^- + H_2 (M = Ca, Mg) - \text{reaction in areas without the oxide layer} \quad \text{(Eq 2)}$$

Table 3 Comparison of electrochemical tests and mass loss studies results of studied metallic glasses

Magnesium-based alloy	Immersion time	Weight loss, g/cm^2	V_{corr} (mm/year) determined by weight loss	V_{corr} (mm/year) determined by electrochemical tests
$Mg_{68}Zn_{28}Ca_4$	After 15 min	0.0	0.0	0.34
	After 2 h	0.002	0.001	0.88
	After 5 h	0.01	0.01	1.19
	After 10 h	0.09	0.07	1.26
$Mg_{64}Zn_{32}Ca_4$	After 15 min	0.0	0.0	0.28
	After 2 h	0.001	0.001	0.51
	After 5 h	0.008	0.01	0.97
	After 10 h	0.04	0.03	1.06

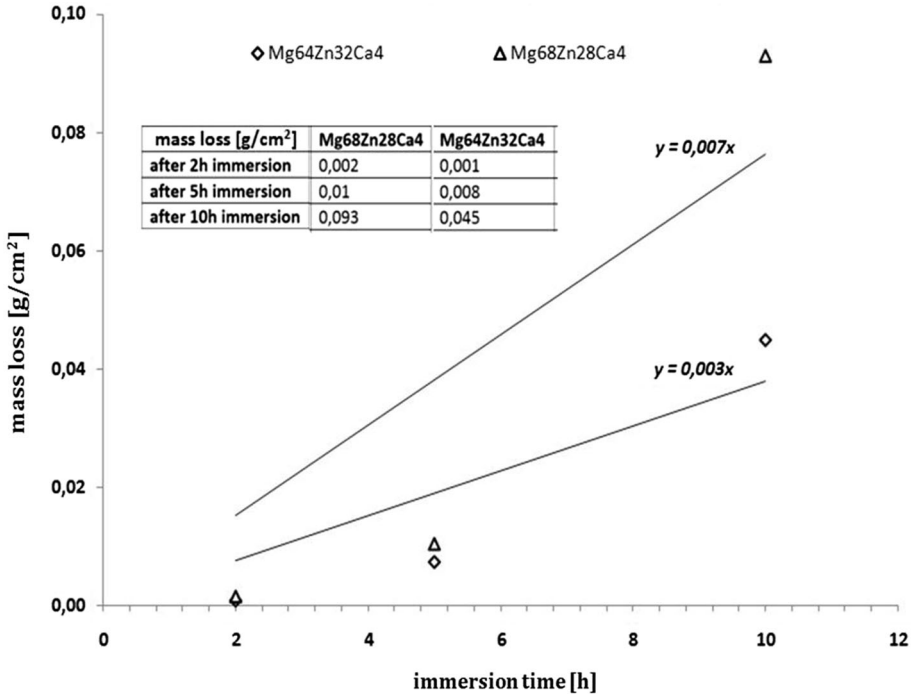

Fig. 9 The weight loss rate of studied $Mg_{68-x}Zn_{28+x}Ca_4$ (x = 0.4) metallic glasses in the Ringer's solution in 37°C

Calcium oxide (CaO) due to high solubility in water (1.65 g/L (Ref 21)) reacts with water and forms calcium hydroxide. Magnesium oxide reacts also with water and forms magnesium hydroxide. Although due to low solubility of MgO (0.08 g/L (Ref 22)), it probably reacts less than CaO. Zinc oxide is not shown in brackets of reaction 1 because it probably did not create zinc hydroxide due to low solubility in water (0.001 g/L (Ref 23)). However, metal ions of Mg, Zn and Ca from reaction 2 according to expression 3 reacted with the hydroxyl groups (OH groups).

$$M^{2+} + 2OH^- \rightarrow M(OH)_2 (M = Mg, Ca, Zn) \quad \text{(Eq 3)}$$

The products of the last reaction 3 acted as a protective layer on the surface of the sample. With the increase in the

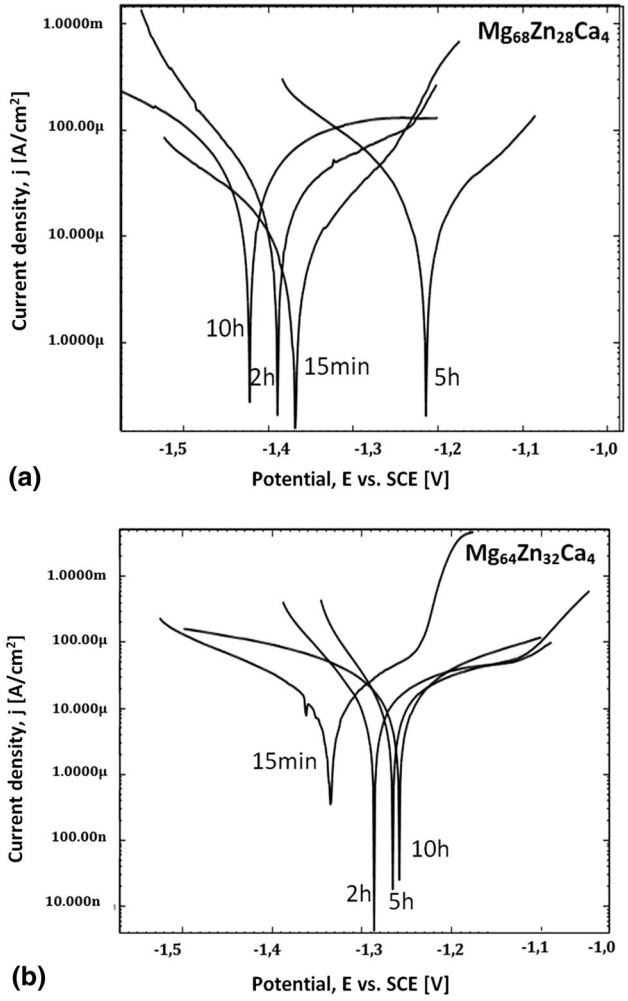

Fig. 10 Potentiodynamic curves of the $Mg_{68}Zn_{28}Ca_4$ (a) and $Mg_{64}Zn_{32}Ca_4$ (b) alloys in Ringer's solution at the 37 °C

immersion time, the protection layer became thicker and caused the decrease in the corrosion rate. Zhu et al. (Ref 24) showed that in the initial stage of immersion in Hank's solution, a layer of $Mg(OH)_2$ grows on the magnesium alloys surface. That is effective protection which reduces the dissolution rate in Hank's solution. According to Pourbaix diagram (Ref 25), the protective layer of magnesium hydroxide $Mg(OH)_2$ is not stable and magnesium hydroxide is dissolved, which leads to the production of Mg cations and anions of OH groups, when the pH is stable at a level of 7.4 (Ref 26).

Penetration of chlorides into the hydroxide layer The magnesium hydroxide layers in this case were porous (Ref 27). The pores in the magnesium hydroxide layer facilitated the surface penetration by chloride ions. A high concentration of chloride ions in Ringer's solution transformed insoluble $M(OH)_2$ to soluble MCl_2 by means of the following reaction:

$$M(OH)_2 + 2Cl^- \rightarrow MCl_2 + 2OH^- (M = Mg, Ca) \qquad \text{(Eq 4)}$$

As a result of this reaction, in the protective layer the phase of composition was changing to MCl_2, which in consequence led to continuous dissolution of Mg-based metallic glasses and penetration of metal ions into the solution (Ref 28).

Release of metal ions and penetration into the solution The released ions of alloying elements reacted with solution components according to their electrochemical activity. The dissolution rate of Mg-based metallic glasses depended on the electrochemical activity of each alloying additive. Dissolution of active magnesium and calcium led to the enrichment of the sample surface with zinc (Table 1 and 2).

Release of hydrogen The corrosion process of Mg-based metallic glasses led also to the release of hydrogen. The hydrogen resulted from reaction (2) and depending on its concentration it could be released or absorbed into the sample (Ref 29).

Formation of a protective layer The corrosion products form a protection layer. Production of the protective layer included three phenomena:

1. Surface enrichment with less active Zn due to the transfer of more active Mg and Ca ions into the solution.
2. Formation of soluble-in-water $Mg(OH)_2$ and/or $Ca(OH)_2$ compounds on the surface of magnesium-based metallic glasses.
3. Formation of the precipitate of calcium carbonate on the surface of the immersed sample.

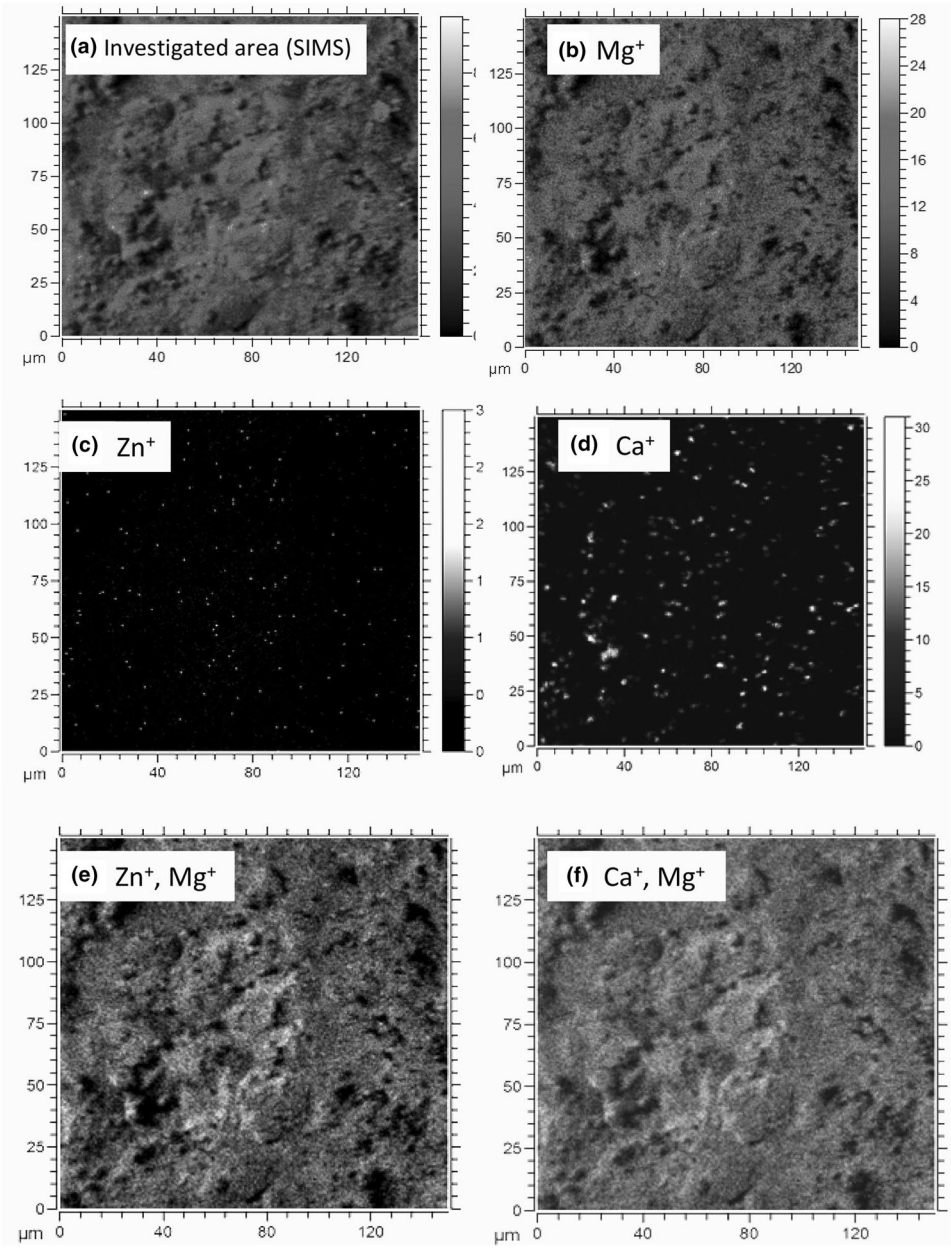

Fig. 11 Results of surface investigations using the SIMS method of $Mg_{68}Zn_{28}Ca_4$ metallic glasses after 24 h of immersion in Ringer's solution: (a) studied micro-area, (b) location of Mg ions, (c) location of Zn ions, (d) location of Ca ions, (e) imposition of Zn and Mg ions and (f) imposition of Ca and Mg ions

In summary, the dissolution rate of the Mg-based metallic glasses in Ringer's solution can be considered as a result of the following processes: the release of corrosion products and the creation of a protective layer.

5. Conclusions

1. The results of corrosion tests showed that the dissolution rate expressed by the volume of released hydrogen de-

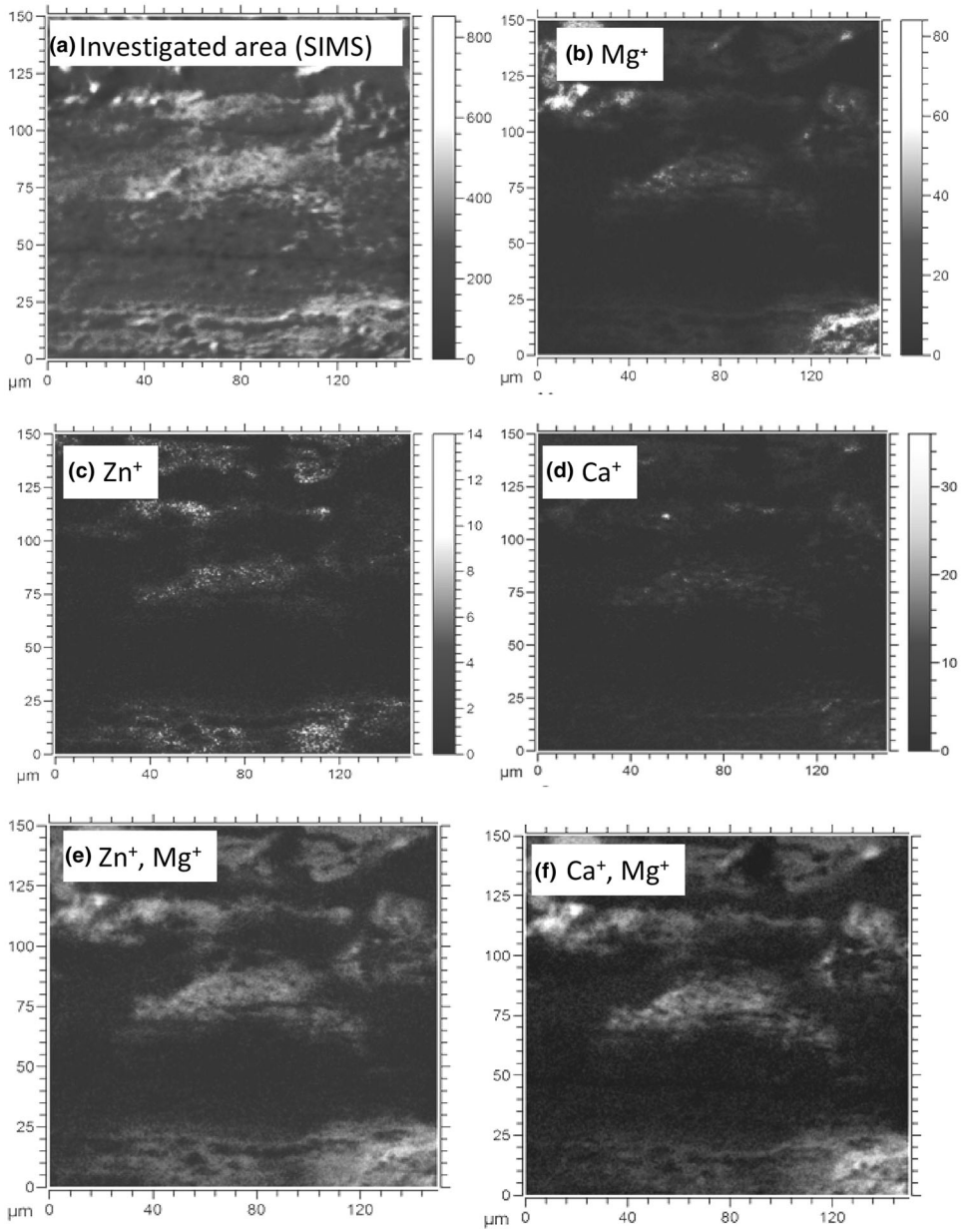

Fig. 12 Results of surface investigations using the SIMS method of $Mg_{64}Zn_{32}Ca_4$ metallic glasses after 24 h of immersion in Ringer's solution: (a) studied micro-area, (b) location of Mg ions, (c) location of Zn ions, (d) location of Ca ions, (e) imposition of Zn and Mg ions and (f) imposition of Ca and Mg ions

creased with the increasing of zinc concentration in the studied magnesium metallic glasses.

2. The corrosion products act as protective layers, which periodically slow down the dissolution process. However, it is mainly the discontinuity of these layers that is responsible for the periodical course of dissolution.
3. The formation of biocompatible corrosion products ($CaCO_3$, MgO, ZnO and ions of Mg, Zn, Ca) during the dissolution of the sample in Ringer's solution and the formation of a protective layer on the surface of the $Mg_{64}Zn_{32}Ca_4$ metallic glass suggest using this alloy as a resorbable material for short-term implants.

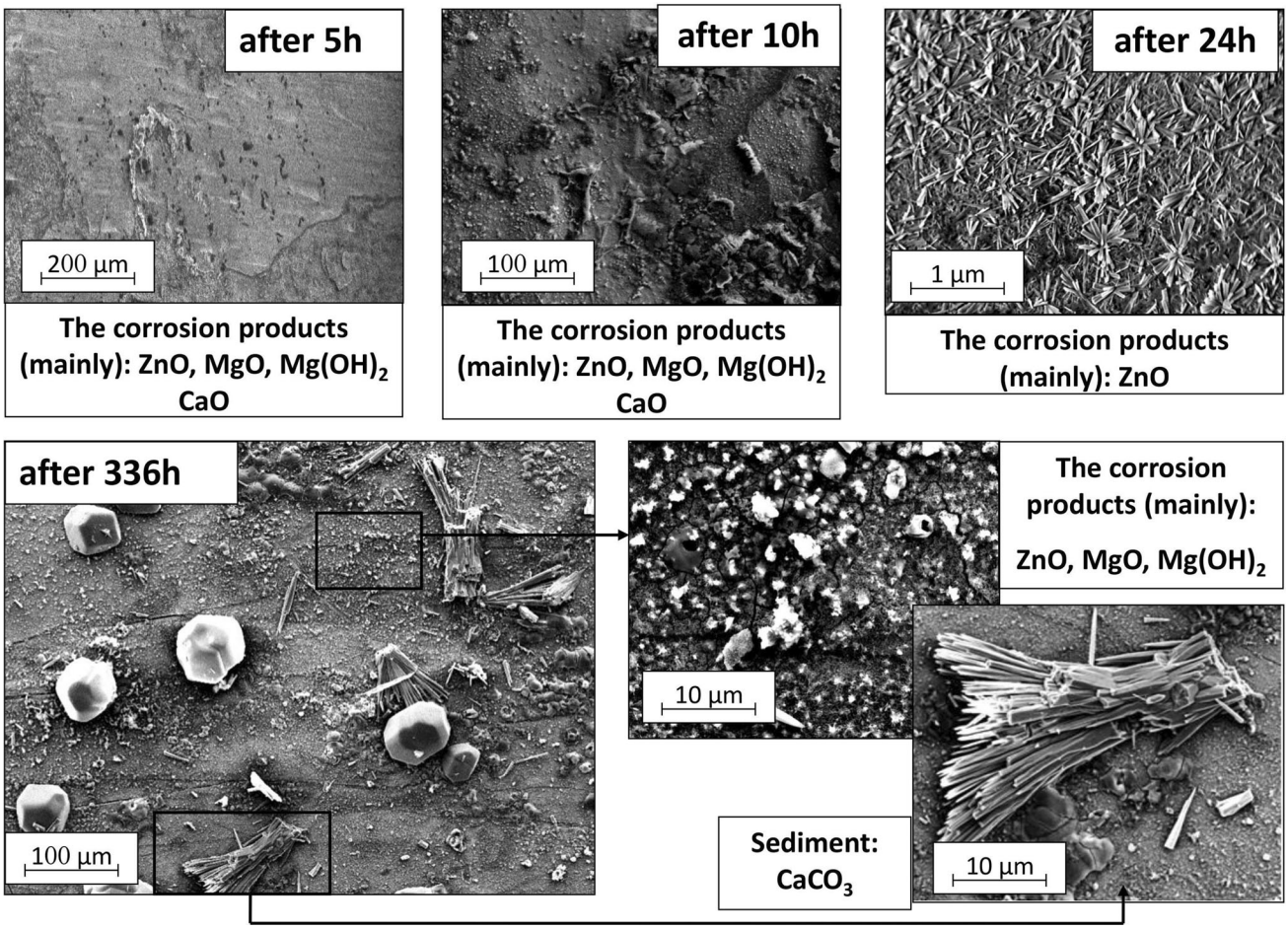

Fig. 13 Corrosion products on the $Mg_{64}Zn_{32}Ca_4$ sample after 5, 10, 24 and 336 h of immersion in Ringer's solution at 37 °C

Acknowledgments

The work was supported by the National Science Centre under research Project No.: 2013/09/B/ST8/02129.

References

1. N. Abidin, B. Rolfe, H. Owen, J. Malisan, D. Martin, J. Hofstetter, P.J. Uggowitzer, and A. Atrens, The In vivo and In vitro Corrosion of High-Purity Magnesium and Magnesium Alloys WZ21 and AZ91, *Corros. Sci.*, 2013, **75**, p 354–366
2. L.P. Xu, G. Yu, E. Zhang, F. Pan, and K. Yang, In vivo Corrosion Behavior of Mg–Mn–Zn Alloy for Bone Implant Application, *J. Biomed. Mater. Res. A*, 2007, **83**(3), p 703–711
3. E. Zhang, W. He, H. Du, and K. Yang, Microstructure, Mechanical Properties and Corrosion Properties of Mg–Zn–Y Alloys with Low Zn Content, *Mater. Sci. Eng. A*, 2008, **488**, p 102–111
4. Y. Wan, G. Xiong, H. Luo, F. He, Y. Huang, and X. Zhou, Preparation and Characterization of a New Biomedical Magnesium–Calcium Alloy, *Mater. Des.*, 2008, **29**, p 2034–2037
5. S. Zhang, J.N. Li, Y. Song, C.L. Zhao, X.N. Zhang, and C. Xie, In vitro Degradation, Hemolysis and MC3T3-E1 Cell Adhesion of Biodegradable Mg–Zn Alloy, *Mater. Sci. Eng. C*, 2009, **29**, p 1907–1912
6. G. Song and S. Song, A Possible Biodegradable Magnesium Implant Material, *Adv. Eng. Mater.*, 2007, **9**, p 221–327
7. J.X. Jia, A. Atrens, G. Song, and T. Muster, Simulation of Galvanic Corrosion of Magnesium Coupled to a Steel Fastener in NaCl Solution, *Mater. Corros.*, 2005, **56**, p 468–474
8. J.W. Chang, X.W. Guo, P.H. Fu, A. Atrens, L.M. Peng, W.J. Ding, and X.S. Wang, A Comparison of the Corrosion Behaviour in 5% NaCl Solution of Mg Alloys NZ30K and AZ91D, *J. Appl. Electrochem.*, 2008, **38**, p 207–2014
9. S. Lesz, R. Babilas, M. Nabialek, M. Szota, M. Dospial, and R. Nowosielski, The Characterization of Structure, Thermal Stability and Magnetic Properties of Fe-Co-B-Si-Nb Bulk Amorphous and Nanocrystalline Alloys, *J. Alloy. Compd.*, 2011, **509**, p 197–201
10. R. Babilas, K. Cesarz-Andraczke, R. Nowosielski, and A. Burian, Structure, Properties, and Crystallization of Mg-Cu-Y-Zn Bulk Metallic Glasses, *J. Mater. Eng. Perform.*, 2014, **23**, p 2241–2246
11. Z. Shi and A. Atrens, An Innovative Specimen Configuration for the Study of Mg Corrosion, *Corr. Sci.*, 2011, **53**, p 226–246
12. A. Atrens, M. Liu, and N.I.Z. Abidin, Corrosion Mechanism Applicable to Biodegradable Magnesium Implants, *Mater. Sci. Eng. B*, 2011, **176**, p 1609–1636
13. Y. Wang, M.J. Tan, J. Pang, Z. Wang, and A.W.E. Jarfors, In vitro Corrosion Behaviors of Mg67Zn28Ca5 Alloy: from Amorphous to Crystalline, *Mater. Chem. Phys.*, 2012, **134**, p 1079–1087
14. B. Zberg, P.J. Uggowitzer, and J.F. Löffler, Towards a New Generation of Biodegradable Implants: MgZnCa Glasses Without Hydrogen Evolution, *Nat. Mater.*, 2009, **8**, p 887–891

15. N. Abidin, A.D. Atrens, D. Martin, and A. Atrens, Corrosion of High Purity Mg, Mg2Zn0.2Mn, ZE41 and AZ91 in Hank's Solution at 37 °C, *Corros. Sci.*, 2011, **53**, p 3542–3556
16. S. Feliu, Jr, and I. Lorente, Corrosion Product Layers on Magnesium Alloys AZ31 and AZ61: Surface Chemistry and Protective Ability, *Appl. Surf. Sci.*, 2015, **347**, p 736–746
17. G. Song, *Corrosion Prevention of Magnesium Alloys*, 1st ed., Woodhead Publishing limited, Philadelphia, 2013
18. P. Dudek, A. Fajkiel, T. Reguła, and K. Saja, Selected Problems of a Technology of the AZ91 Magnesium Alloy Melt Treatment, *Res. Inst. Foundry*, 2009, **1**, p 27–42 (in Polish)
19. K. Asami and S. Ono, Quantitative X-ray Photoelectron Spectroscopy Characterization of Magnesium Oxidized in Air, *J. Electrochem. Soc.*, 2000, **147**, p 1408–1413
20. M. Santamaria, F. DiQuarto, S. Zanna, and P. Marcus, Initial Surface Film on Magnesium Metal: A Characterization by X-ray Photoelectron Spectroscopy (XPS) and Photocurrent Spectroscopy (PCS), *Electrochim. Acta*, 2007, **53**, p 1315–1325
21. A Safety Data Sheet of CaO (in Polish). http://www.poch.com.pl/1/wysw/utworz_pdf.php?nr_karty=1353
22. A Safety Data Sheet of MgO (in Polish). http://www.poch.com.pl/1/wysw/utworz_pdf.php?nr_karty=750
23. A Safety Data Sheet of ZnO (in Polish). http://www.poch.com.pl/1/wysw/msds_clp.php?A=5497e8d254127b4a0001
24. Y. Zhu, G. Wu, Y.H. Zhang, and Q. Zhao, Growth and Characterization of $Mg(OH)_2$ Film on Magnesium Alloy AZ31, *Appl. Surf. Sci.*, 2011, **257**, p 6129–6137
25. J. Baszkiewicz and M. Kamiński, *Fundamentals of Metal Corrosion*, 1st ed., Polish Scientific Publishing, Warsaw, 1997 (in Polish)
26. M. Salahshoor and Y. Guo, Biodegradable Orthopedic Magnesium-Calcium (MgCa) Alloys, *Process. Corros. Perform. Mater.*, 2012, **5**, p 135–155
27. M. Liu, P. Schmutz, P.J. Uggowitzer, G. Song, and A. Atrens, The Influence of Yttrium (Y) on the Corrosion of Mg–Y Binary Alloys, *Corros. Sci.*, 2010, **52**, p 3687–3701
28. F. Rosalbino, S. De Negri, A. Saccone, E. Angelini, and S. Delfino, Bio-corrosion characterization of Mg–Zn–X (X = Ca, Mn, Si) alloys for biomedical applications, *J. Mater. Sci. Mater. Med.*, 2010, **21**, p 1091–1098
29. N. Abidin, A.D. Atrens, D. Martin, and A. Atrens, Corrosion of High Purity Mg, Mg2Zn0.2Mn, ZE41 and AZ91 in Hank's Solution at 37 °C, *Corros. Sci.*, 2011, **53**, p 3542–3556